JOURNAL OF GUIDANCE, CONTROL, AND DYNAMICS
Vol. 18, No. 3, May–June 1995

Three-Dimensional Air-to-Air Missile Trajectory Shaping

Renjith R. Kumar* and Hans Seywald*
Analytical Mechanics Associates, Inc., Hampton, Virginia 23666-1398
and
Eugene M. Cliff† and Henry J. Kelley‡
Virgina Polytechnic Institute and State University, Blacksburg, Virginia 24061

Open-loop range/energy/time optimal trajectories are synthesized for a three-dimensional point-mass model of a boost–sustain–coast air-to-air missile (AAM) in atmospheric flight. Boundaries of attainable sets for various fixed flight times are obtained by numerically solving the associated two-point boundary value problem (TPBVP) implied by the first-order necessary conditions of optimal control. The attainable set provides insight into the range capabilities of the missile in all directions in the down range–cross range plane for prescribed end-game energy requirements. Necessary and sufficient conditions for optimality are checked for candidate extremals. A *new* governing matrix differential equation and suitable boundary conditions are derived to check for conjugate points along *regular* or *regularized* extremals. This new matrix differential equation overcomes the difficulty of standard matrix Riccati equations for conjugate point testing, which have components whose values go to infinity even in the absence of conjugate points. The open-loop solutions presented in this study can be utilized to generate a neighboring near-optimal guidance scheme.

Introduction

EARLIER work on trajectory shaping and guidance for medium range air-to-air missiles (AAMs) were in general performed with ideas of singular perturbation theory[1–3] using reduced-order modeling. Guidance schemes using these theories were compared to existing linear optimal solutions or to proportional navigation. In two-dimensional atmospheric flight in the vertical plane, a point-mass model of a boost–sustain–coast AAM has been used and results[4] show the poor correlation between the solutions of point-mass models and reduced-order models (Ref. 4, p. 56). The above reason prompted the departure to a more realistic three-dimensional point-mass model, the ultimate aim being to obtain a near-optimal closed-loop guidance algorithm.[5]

Various problems such as the minimum time to intercept, maximum launcher range at launch, maximum range of missile, maximum launcher range at intercept, etc., have been studied in earlier works.[4,6] Depending upon details of the target type, the maximization parameter may vary. For example, it may be important to stay outside the reach of the target's air defense weaponry so that the stand-off distance is important.

In the present research, a specific problem is examined, namely, to obtain the boundary of attainable range of a given missile for various end conditions. For arbitrary but fixed flight times, the boundary of attainability consists of the maximum- and minimum-range points in the horizontal plane. Each point along the boundary of the set of attainability represents an optimal range intercept trajectory for specified initial and terminal conditions for fixed final time. Thus, the attainable sets and their maximum-range intercept points are of direct consequence for a guidance scheme development. Furthermore, the attainable sets, or "foot-prints," provide valuable insight into the capabilities of the missile for the given thrust and weight configuration.

The vehicle model used in this study assumes vertical and horizontal load factors as the two control variables. The controls are bounded by structural and aerodynamic limits. The atmospheric model used is realistic and the aerodynamic model of the missile shows altitude and Mach number dependency of the drag. The propulsion system is of boost–sustain–coast type with fixed switching times and fixed thrust magnitudes on each arc.

The numerical solution of the two-point boundary value problem (TPBVP) was performed by using the multiple-shooting algorithm BOUNDSCO[7] modified for the specific purpose. The initial guesses required for solving the TPBVP were obtained from solutions in the vertical plane.[4] Comparisons of state and control trajectories leading to maximum- and minimum-range boundary points are made. Trajectories for typical flight times and altitude and energy corridors are computed.

The homotopy or continuation methods used to obtain the boundary of attainability sets uses an array of homotopy parameters, and the transition between these parameters is explained in detail. Abnormal points encountered during the continuation method can be overcome only by careful choice of the homotopy parameters. The nonconvexity of the attainability sets and the appearance of "holes" or unreachable points within the boundary of attainability delineates the range capabilities of the AAM.

Once the boundary value problem is solved, with the control variables satisfying the Pontryagin minimum principle, the second-order necessary and sufficient conditions were tested. The regular and regularized extremals were subject to conjugate point testing using ideas of neighboring optimal solutions.[8] In standard literature,[8] the finiteness of a certain composite matrix whose components are obtained by solving governing matrix differential equations is equivalent to the nonexistence of conjugate points. The finite escape time of the submatrices obtained by integration does not necessarily imply the same for the composite matrix used to check conjugate points. A differential equation for the composite matrix and suitable boundary conditions have been derived in this paper so that the above-mentioned impasse is overcome.

Problem Formulation

The nominal optimal control problem is to obtain the boundary of attainability of the missile in the horizontal projection for fixed final time with the other states fixed or unprescribed. The following assumptions are made: 1) point-mass model; 2) flat earth; 3) three-dimensional missile trajectory; 4) air density that varies with altitude; 5) drag that is a function of altitude, Mach number, and control effort; and 6) thrust and weight histories that are predetermined functions of time.

Presented as Paper 89-3637 at the AIAA Guidance, Navigation, and Control Conference, Boston, MA, Aug. 14–16, 1989; received Nov. 12, 1992; revision received April 15, 1994; accepted for publication Sept. 25, 1994.

*Supervising Engineer. Member AIAA.
†Reynolds Metal Chaired Professor, Department of Aerospace and Ocean Engineering. Fellow AIAA.
‡Late Chaired Professor, Department of Aerospace and Ocean Engineering. Fellow AIAA.

The equations of motion for the three-dimensional point-mass model of the missile are as follows:

$$\begin{aligned} \dot{x} &= V\cos\gamma\cos\chi \\ \dot{y} &= V\cos\gamma\sin\chi \\ \dot{h} &= V\sin\gamma \\ \dot{E} &= [T - D(h, M, n)](V/W) \\ \dot{\gamma} &= (n_v - \cos\gamma)\frac{g}{V} \\ \dot{\chi} &= \frac{n_h}{\cos\gamma}\frac{g}{V} \end{aligned} \tag{1}$$

where x is the down range of the missile, y the cross range, h the altitude, and E the specific energy. The velocity is obtained from the algebraic equation $V = \sqrt{2g(E-h)}$. The flight-path angle is γ, and χ denotes the heading angle. The parameter T is the thrust magnitude, D the aerodynamic drag, W the weight of the missile, and M the Mach number. The two controls are n_v, the vertical load factor, and n_h, the horizontal load factor. The resultant load factor is obtained from the algebraic expression $n = \sqrt{(n_v^2 + n_h^2)}$.

The variations of drag with altitude, Mach number, and load factor are given by the following set of equations:

$$\frac{D}{W}(h, M, n) = D_0 + D_i n^k \tag{2}$$

where

$$D_0 = \frac{qS}{W}C_{D0}(h, M) \tag{3}$$

$$D_i = \left(\frac{qS}{W}\right)^{1-k} C_{Di}(M) \tag{4}$$

A good approximation of $C_{D0}(h, M)$ is obtained by the empirical formula

$$C_{D0}(h, M) = \hat{C}_{D0}(M)\left[1 + a\left(\frac{h}{h_m}\right)^m\right] + C_{DC}(M)f(T) \tag{5}$$

Here, $q = 0.5\varrho(h)V^2$ is the dynamic pressure, S the characteristic surface area, and $\varrho(h)$ the air density. The term C_{D0} is the zero-lift drag coefficient and $\hat{C}_{D0}$ is the component independent of altitude, C_{Di} denotes the induced drag coefficient and C_{DC} the base drag coefficient, and $f(T)$ is the power on–off designator, i.e., $f(T) = 0$ if thrust is on and $f(T) = 1.0$ if thrust is off. Furthermore, $k = 1.8$, $m = 1.833$, $a = 1.7742$, and $h_m = 200{,}000$ ft.

The control variables are limited by two constraints:

Structural limit

$$n(t) \le n_{\max}$$

Aerodynamic limit

$$n(t) \le n_L \doteq C_{L,\max}(M)\frac{qS}{W}$$

The drag coefficients and atmospheric data are all approximated by cubic splines, as is the $C_{L,\max}$ limit. The thrust dependence on altitude is neglected. The values for structural limit, drag polar coefficient, thrust magnitudes, and boost–sustain–coast switching times have been selected from the two-dimensional study.[4] The thrust and weight histories are shown in Figs. 1 and 2, respectively.

The launcher aircraft is assumed to be cruising at a prescribed altitude with a given velocity. It is also assumed that no prelaunch maneuver is performed. The initial flight-path angle and the heading angle are assumed to be zero. The initial velocity of the missile is the same as the initial velocity of the launcher. The control parameter histories are to be determined to obtain the attainable set boundary points in the x–y plane for a given final time. The final altitude of the missile is prescribed to be the nominal final altitude of the target. The intercept is to be achieved with a prescribed lower bound on the final energy, so that during real-time guidance the final velocity of the missile will be sufficiently high for end-game maneuvers. The final orientation angles of the velocity vector are not prescribed.

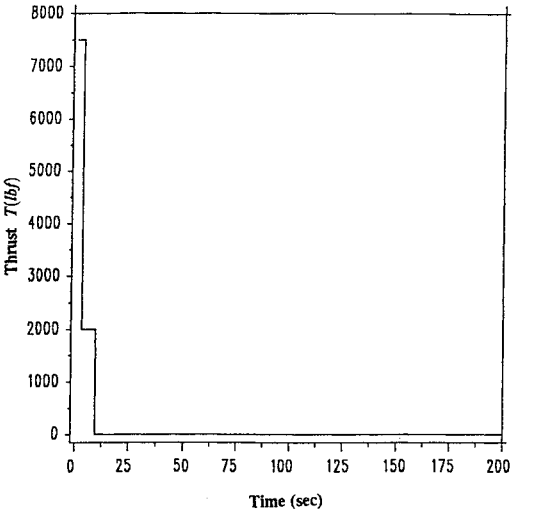

Fig. 1 Thrust time history of missile.

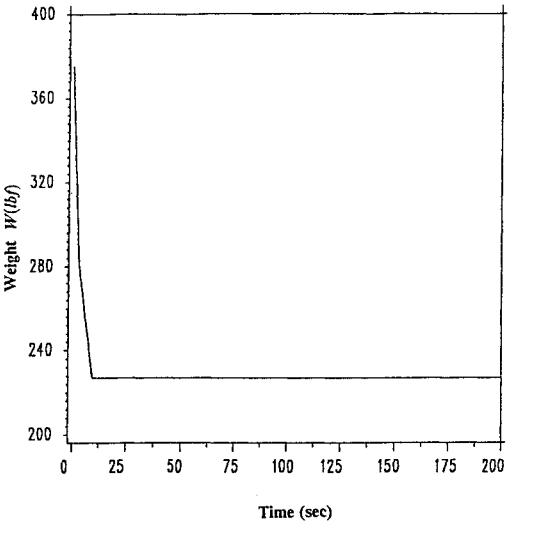

Fig. 2 Weight time history of missile.

The resulting boundary conditions for the intercept problem are as follows:

Initial conditions

$$x(t_0) = 0, \quad y(t_0) = 0, \quad h(t_0) = h_0$$

$$E(t_0) = E_0, \quad \gamma(t_0) = 0, \quad \chi(t_0) = 0$$

Final conditions

$$\boxed{\begin{aligned} x(t_f) &= x_{\max/\min} \\ y(t_f) &= y_{\text{fixed}} \end{aligned}} \quad \text{or} \quad \boxed{\begin{aligned} x(t_f) &= x_{\text{fixed}} \\ y(t_f) &= y_{\max/\min} \end{aligned}}$$

$$h(t_f) = h_f, \quad E(t_f) \ge E_f, \quad \gamma(t_f) = \gamma_{\text{free}}$$

$$\chi(t_f) = \chi_{\text{free}}$$

The above boundary conditions indicate range maximization/minimization in all directions in the x–y plane for other states specified or free. This problem is denoted as problem $\boldsymbol{p}_1$. The initial conditions of down range and cross range can always be chosen as zero, since these do not appear on the right-hand side of the differential equations. The final orientation angles are free and the angles are assumed to be zero at launch. Hence, the flooding of state space requires a seven-parameter $(h_0, h_f, E_0, E_f, x(t_f), y(t_f), t_f)$ family

of solutions. The solutions of the above optimal control problem for fixed initial and final values of altitude and energy is termed a range chart, which contains the maximum- and minimum-range intercept points for various final times. Thus it is clear that a four-parameter family (h_0, h_f, E_0, E_f) of such charts is to be generated for flooding the entire state space.

The initial and final altitudes of the missile can vary from 0 ft to approximately 50,000 ft, since these are the nominal flying altitude corridors for the high-performance fighter aircraft assumed in this study. The study reported in Ref. 4 indicates that neighboring guidance in the vertical plane can be achieved with large initial altitude perturbations (on the order of 5000 ft). This implies that the discretization mesh for initial and final altitudes can be coarse (nine discretization nodes each). Similar results[4] for the initial and final energy of the missile (or the launcher velocity and end-game velocity requirements) make the number of "range charts" required for real-time on-board guidance reasonable.

Optimal Control Logic

The usual variation-based approach to these problems proceeds with construction of a Hamiltonian function and application of the minimum principle.[9,10] However, before proceeding with such a theory of necessary conditions, it is prudent to establish the existence of a solution for the given optimal control problem. One key condition in the existence theory[11] is the convexity of the hodograph[12,13] or velocity set in the state-rate space. For the problem at hand, the controls appear only in three components of the state equations, and hence the hodograph is three dimensional. Figure 3 shows a three-dimensional hodograph for the present problem at specified states and times. The hodograph comprises only of the surface and not the volume and hence is nonconvex. However, this can be overcome by relaxation of the controls,[11–13] i.e., by adding points to the maneuverability domain such that the hodograph of the relaxed problem is equal to the convex hull of the hodograph of the original problem. An easy method of convexizing the hodograph for the specific problem is to introduce an additional control in the differential equations similar in physical nature to speed brake. Explicity, this leads to

$$\dot{E} = (V/W)[T - \varkappa(D - D_{\max}) - D_{\max}] \tag{6}$$

where $\varkappa$ is the additional control variable in the form of a speed brake. Here, $D_{\max}$ is the maximum drag possible and is a function of altitude and velocity of the missile whereas D is a function of altitude, velocity, and the control variables. Here, $\varkappa \in [0, 1]$ convexizes the hodograph; $\varkappa = 1$ indicates the original hodograph surface and

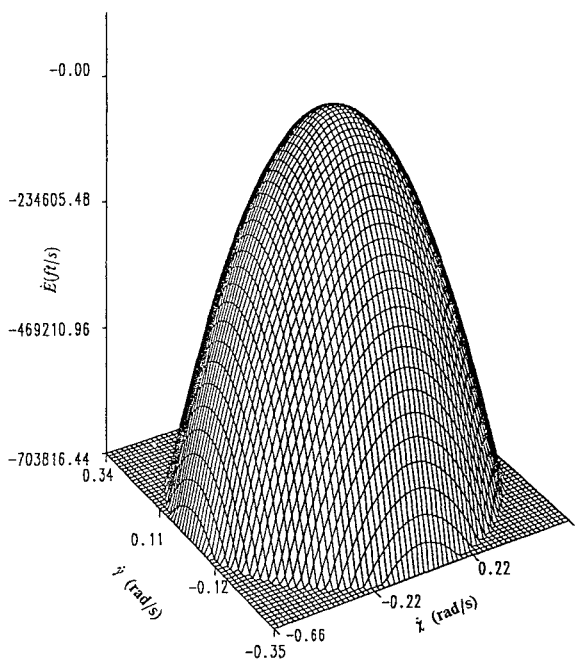

Fig. 3 Hodograph space.

$\varkappa = 0$ "closes the lid" or forms the convex hull. Any other value of $\varkappa$ denotes a point inside the convexized hodograph. The surface of the paraboloid shown in Fig. 3 is the hodograph space of the unrelaxed problem, whereas the entire volume becomes the hodograph space for the relaxed problem. Values of $\varkappa$ not equal to unity are singular solutions of the relaxed problems. These singular solutions correspond to chattering solutions of the original nonrelaxed problem. It should be mentioned here that operation in the nonconvex regions of the hodograph space for this specific range optimization problem is analogous to operating at high drag (waste of energy), which is clearly of little interest. This is analyzed later, following the definition of adjoint variables and transversality conditions.

The "minimum" principle is consistently followed in this analysis. The variational Hamiltonian is defined as follows:

$$H \equiv \sum \lambda_i \dot{X}_i \tag{7}$$

where the λ_i, $i = 1, \ldots, 6$, are the costate or adjoint variables and the X_i, $i = 1, \ldots, 6$, are the state variables. To account for control bounds, it is convenient to augment Eq. (7) and define the augmented Hamiltonian as

$$\hat{H} \equiv \sum \lambda_i \dot{X}_i + \mu_1(n - n_{\max}) + \mu_2\left(n - C_{L,\max}(M)\frac{qS}{W}\right)$$

where μ_1 and μ_2 are the multipliers, commonly called the Valentine multipliers, corresponding to the control constraints. A particular multiplier is equal to zero if the respective constraint is inactive and may be greater than zero if the respective constraint is active. This nature of the Valentine multipliers results from the Kuhn–Tucker conditions.[8]

The Euler–Lagrange equations provide the differential system of costate variables:

$$\dot{\lambda}_i = -\frac{\partial \hat{H}}{\partial X_i} \tag{8}$$

The optimal values of the control variables are determined from the Pontryagin minimum principle; i.e., minimize the variational Hamiltonian subject to the control constraints. If the controls are in the interior of the control constraint set, then

$$\frac{\partial H}{\partial n_v} = 0, \qquad \frac{\partial H}{\partial n_h} = 0 \tag{9}$$

For this unconstrained case, the optimal controls are given by the formulas

$$n_v^* = -\text{sgn}(\lambda_\gamma)\left|\frac{\lambda_\gamma g}{[\lambda_E D_i V^2 k]}\right|^{1/(k-1)} \times \left[\left(\frac{\lambda_\chi}{\lambda_\gamma \cos\gamma}\right)^2 + 1\right]^{(1-k/2)/(k-1)} \tag{10}$$

$$n_h^* = -\text{sgn}(\lambda_\chi)\left|\frac{\lambda_\chi g}{[\lambda_E D_i V^2 k \cos\gamma]}\right|^{1/(k-1)} \times \left[\left(\frac{\lambda_\gamma \cos\gamma}{\lambda_\chi}\right)^2 + 1\right]^{(1-k/2)/(k-1)} \tag{11}$$

If one of the constraints is active, then

$$n_v^* = \frac{-\lambda_\gamma \text{infimum}(n_L, n_{\max})}{[(\lambda_\chi/\cos\gamma)^2 + \lambda_\gamma^2]^{0.5}} \tag{12}$$

$$n_h^* = \frac{-\lambda_\chi \text{infimum}(n_L, n_{\max})}{\cos\gamma[(\lambda_\chi/\cos\gamma)^2 + \lambda_\gamma^2]^{0.5}} \tag{13}$$

The weak form of the classical Legendre–Clebsch condition for the unconstrained minimizing extremal requires that

$$[H_{uu}] \geq 0 \tag{14}$$

i.e., the Hessian matrix with respect to the control vector $u = [n_v\ n_h]^T$ be positive semidefinite. This implies that the diagonal elements must be nonnegative, i.e.,

$$\frac{\partial^2 H}{\partial n_v^2} \geq 0, \qquad \frac{\partial^2 H}{\partial n_h^2} \geq 0 \tag{15}$$

The above equations yield the necessary conditions that, for the unconstrained case, $\lambda_E \leq 0$ and n_v and n_h not be zero simultaneously. It can also be verified that the determinant of the matrix H_{uu} is nonnegative.

In this connection one traces back to the hodograph space. It is clear that the optimal state rate and the associated optimal controls are determined uniquely by the minimum principle unless $\lambda_E \geq 0$ and λ_γ and λ_χ are simultaneously equal to zero. If this situation occurs along a nonzero time interval, then the optimal control is called singular.[8] If λ_E is equal to zero along with the other two costates λ_γ and λ_χ, the minimum principle is vacuous. If $\lambda_E > 0$ with λ_γ and λ_χ both zero, the plane of constant minimizing Hamiltonian becomes parallel to the elliptical base of the convexized hodograph space. The relaxed problem would give a singular control solution for the load factors that would correspond to the chattering nature of the original unrelaxed problem. Thus, for nonchattering phenomena for all possible λ_γ and λ_χ, one must operate only in the domain of a negative λ_E. This corresponds to an energy conservative system. If, on the other hand, the energy multiplier is positive, the $\varkappa$ parameter representing speed brake would be zero, corresponding to increased drag operation.

Transversality Conditions

The final energy of the missile should be greater than or equal to a specified value. In practice, while using indirect methods, the optimal control problem is first solved with $E(t_f)$ specified. If the obtained value of $\lambda_E(t_f)$ is less than or equal to zero, the solution is accepted. If $\lambda_E(t_f) > 0$, one must re-solve the problem with a natural boundary condition $\lambda_E(t_f) = 0$. Here, $\lambda_E(t_f) > 0$ indicates that the specified value of $E(t_f)$ is less than the "natural" value.

The final-flight path angle and the final heading angle are unspecified and hence the associated costates λ_γ and λ_χ are zero at final time. The final angles may also be specified, if necessary. The unspecified final angles give rise to a "nonregular" problem for which the strengthened form of the classical Legendre–Clebsch condition does not hold at final time since λ_γ and λ_χ are zero at final time. Thus sufficiency conditions for a weak local minima cannot be obtained. This is discussed in more detail in the section on necessary and sufficient conditions for optimality.

The solution to the TPBVP is approached by fixing $y(t_f)$ and maximizing/minimizing $x(t_f)$ or vice-versa depending upon the region of homotopy in order to keep the costates bounded. Either $|\lambda_x|$ or $|\lambda_y|$ can be scaled to unity, depending on the region of homotopy.

The Hamiltonian is not an explicit function of time in the coasting arc. Hence H is a constant along the coasting arc, and the value of this constant depends on the final time. The Hamiltonian exhibits jump discontinuities at the thrust switches and varies continuously along the thrust phase.

Numerical Solution

Solution of TPBVP

The aerodynamic data, control bounds, and thrust history for the AAM have been adopted from the two-dimensional study.[4] A sample of the initial and final values of the state variables for a fixed terminal time of 150 s would be as follows:

$$x(t_0) = 0 \text{ ft}, \qquad x(t_f) = x_{\max/\min}$$

$$y(t_0) = 0 \text{ ft}, \qquad y(t_f) = 200{,}000 \text{ ft}$$

$$h(t_0) = 20{,}000 \text{ ft}, \qquad h(t_f) = 20{,}000 \text{ ft}$$

$$E(t_0) = 52{,}800 \text{ ft}, \qquad E(t_f) \geq 140{,}000 \text{ ft}$$

$$\gamma(t_0) = 0 \text{ rad}, \qquad \gamma(t_f) = \gamma_{\text{free}}$$

$$\chi(t_0) = 0 \text{ rad}, \qquad \chi(t_f) = \chi_{\text{free}}$$

Once the TPBVP is formulated, the solution to the optimal control problem is attempted using the nonlinear multipoint boundary value problem solver software BOUNDSCO.[7] This procedure requires good initial guess values of the trajectory (states and costates). The final times were varied from 100 to 225 s. The former time is an ad hoc threshold for medium-range flight and the latter corresponds to the "natural" time for the range maximization problem for values of initial and final altitude and energy specified as before. The final energy requirement for a flight time of 150 s can be varied from 106,100 to 150,000 ft. These correspond to the lower and upper limits beyond which a solution is not possible. The lower limit corresponds to a specified value of final energy less than the natural value (operation below this limit would result in chattering subarcs).

Homotopy Methods

The solution to the vertical plane problem with zero cross-range and heading angle histories is used as an initial guess for point 1 in Fig. 4 (where $\hat{x} = x/20{,}000$ ft and $\hat{y} = y/20{,}000$ ft are nondimensionalized distances). The parameter $y(t_f)$ is used as the initial homotopy parameter, varying $y(t_f)$ from zero to increasing values. Negative values of $y(t_f)$ give symmetric solutions about the downrange axis. The down range at final time $x(t_f)$ is maximized, and hence its costate is fixed at negative unity. Homotopy with $y(t_f)$ is continued until point 2 in Fig. 4. This point corresponds to the terminal surface, which yields $\lambda_y \approx -1$. Continuation of homotopy with $y(t_f)$ would considerably slow the convergence of the continuation technique and would eventually halt the convergence at point 3, corresponding to $\lambda_y \to \infty$. Thus at point 2, the homotopy parameter is changed from $y(t_f)$ to $x(t_f)$. This implies maximizing $y(t_f)$ with $x(t_f)$ fixed. This helps to rescale the multipliers to keep the costate of cross range bounded. From point 2 to point 3, the costate $\lambda_y = -1$ and λ_x changes from approximately -1 to zero at point 3. From point 3 to point 4 the multiplier λ_x increases from zero to unity. Point 4 is characterized by $\lambda_x = +1$ and $\lambda_y = -1$. If the attainable set is strictly convex, then there exists a unique support plane with a unique outward normal at every point on the boundary.[14] The multipliers λ_x and λ_y are related to the slope of the outward normal. This gives a general idea as to the boundedness of each costate multiplier along the homotopy procedure.

It should be noted here that homotopy in a given state is also equivalent locally to a homotopy in its costate. At point 4, the homotopy parameter is changed to λ_y [or $y(t_f)$]. This is to enhance convergence, anticipating the boundary of attainability to become parallel to the cross-range axis, which happens at point 5. This corresponds to $\lambda_x(t_f) = +1$ and $\lambda_y = 0$.

From point 5, the homotopy was continued with $y(t_f)$, with λ_y increasing from zero to a positive quantity and λ_x scaled to $+1$. It was observed that the continuation method failed between point 5 and point 6 due to the sudden transition of λ_y from zero at point

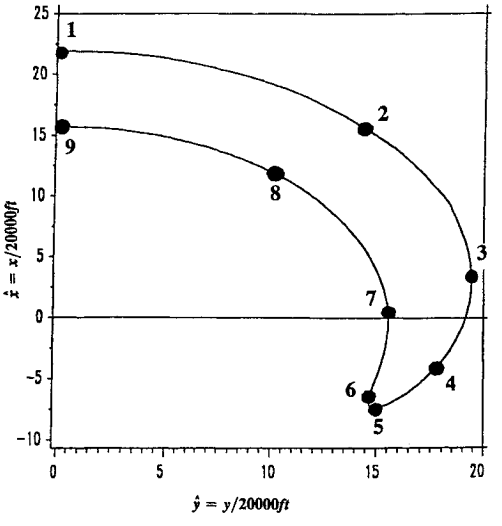

Fig. 4 Attainable set for $t_f = 150$ s.

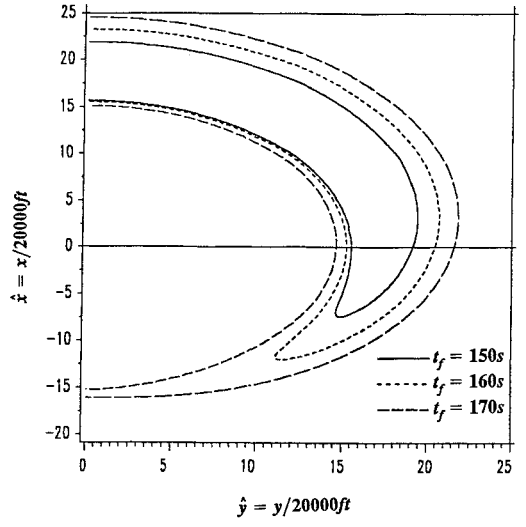

Fig. 5 Attainable set for t_f values of 150, 160, and 170 s.

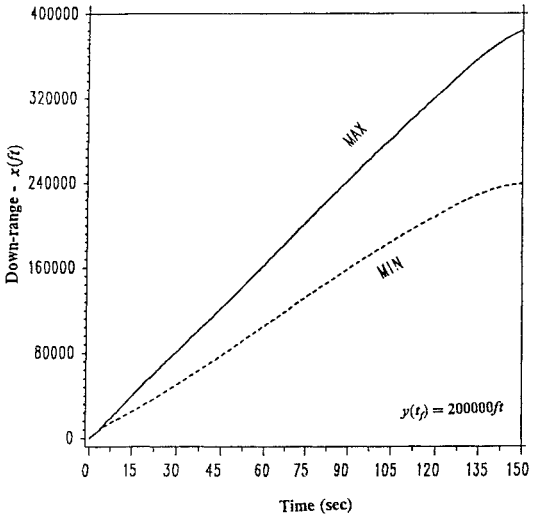

Fig. 6 Down-range time history.

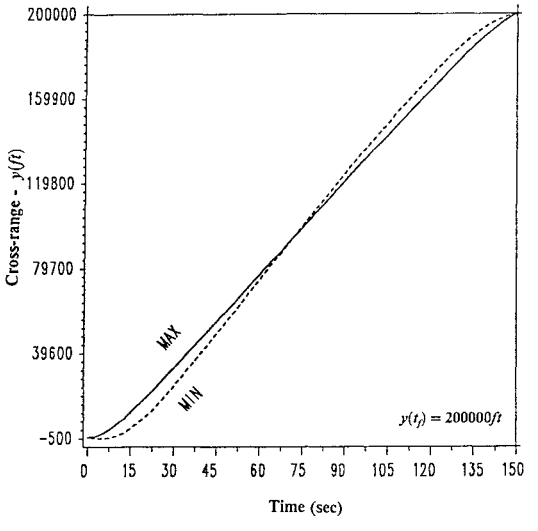

Fig. 7 Cross-range time history.

5 to $+\infty$ at point 6. A change in homotopy parameter to cross range or its costate did not alleviate the convergence problem. This cul-de-sac was circumvented by using Mayer reciprocity.

A minimum-time problem ($\boldsymbol{p}_2$) is solved, fixing $x(t_f)$ and $y(t_f)$. The rescaling of the original problem $\boldsymbol{p}_1$ is performed such that $H(t_f) = -1$. Then for fixed final down range, $y(t_f)$ is varied in such a fashion that the final time corresponding to the isochrone being completed is enclosed within prescribed lower and upper bounds of final time. These bounds are squeezed as much as needed, and the resulting solutions (suitably rescaled) are used as initial guesses to obtain solutions to fixed final-time problem $\boldsymbol{p}_1$. This method is used from point 5 to point 6. The Mayer reciprocity holds for fixed terminal-time extremals with $H(t_f) < 0$. Thus the range optimization problem $\boldsymbol{p}_1$ is equivalent to the minimum-time problem $\boldsymbol{p}_2$ except for pathological cases. Here, $H(t_f) = 0$ would correspond to a pathological case, which is abnormal.

Continuation of the attainability set boundary is performed by varying $x(t_f)$ from point 6 to point 8. Point 7 indicates $\lambda_x = 0$. Point 8 suggests a change in homotopy parameter to $y(t_f)$ to ease the convergence until point 9. The boundary of attainability shown in Fig. 4 has a mirror image about the x axis. Once the boundary is obtained for one isochrone, the procedure can be repeated for different final times, as shown in Fig. 5. It is to be noted that the homotopy can also be performed with cartesian coordinates x and y replaced by polar coordinates R and θ by maximizing or minimizing range R for fixed values of θ. The maximum- and minimum-range arcs would meet at a point beyond which one cannot increase θ for the homotopy. This would indicate an abnormal point. The intricate switching of homotopy parameters required to completely portray the boundary of the attainable set is of clear interest to practicing engineers involved in trajectory optimization.

Attainability Set

The attainable sets and the boundary are shown for different final times in Fig. 5. For a final time of 150 s, the attainability set is closed and nonconvex and does not have any holes. This set is for a fixed value of initial and final altitudes and energy. It has been verified that if the prescribed final energy is decreased, then the maximum range is increased and the minimum range is decreased, thus increasing the area enclosed by the set of attainability. At a given point on the boundary, the local effect of a change in the $E(t_f)$ bound is predicted by the sign of $\lambda_E(t_f)$ [$\lambda_E(t_f) < 0$ implies an expanding boundary as $E(t_f)$ is decreased]. The energy bound at t_f is active for all points on the $t_f = 150$ s boundary. The final energy requirement specification depends upon the target data and the thrust-to-weight ratio of the missile.

As t_f is increased, the same structure of attainability can be observed for flight times up to 169.8 s. These numerics are for initial and final altitudes and energy as specified earlier. For flight time above 169.8 s the maximum- and minimum-range intercept points are "separated." The attainability set is nonconvex and closed but shows the presence of a hole within the set. The area of this hole reduces for larger prescribed flight times.

The above structure of attainability sets is only observed for sufficiently long flight times as used by a medium-range missile. It should be clearly understood that if the missile were to fly coaltitude with the target, as it would if guided by proportional navigation, the final energy would be attained in a very short time (in the order of 25 s) due to high-drag operation. Thus, for very short times it is likely that there exists another family of solutions drastically different in nature from those displayed in this paper. However, the interest here is in medium-range intercepts and the short-range trajectories are not considered.

The set of attainability is used to assess the capabilities of the missile. An example illustrates the use of the attainability set. If a target aircraft is flying toward the launcher aircraft with the line-of-sight vector being 180 deg from the launcher aircraft, then it is clear from the range charts that an intercept with prescribed final energy of 140,000 ft cannot be achieved in 150 or 160 s, whereas there exists a small range corridor if final intercept time is extended to 170 s. This would mean that an earlier detection of the enemy aircraft in pursuit flight is required in order to achieve intercept. The maximum-range boundaries are of clear interest and the associated trajectories are to be stored for near-optimal neighboring guidance.[5]

A detailed comparison is given for a maximum- and a minimum-down-range trajectory for fixed final values of cross range. Figures 6–13 show the state and control histories for $\boldsymbol{p}_1$ using the

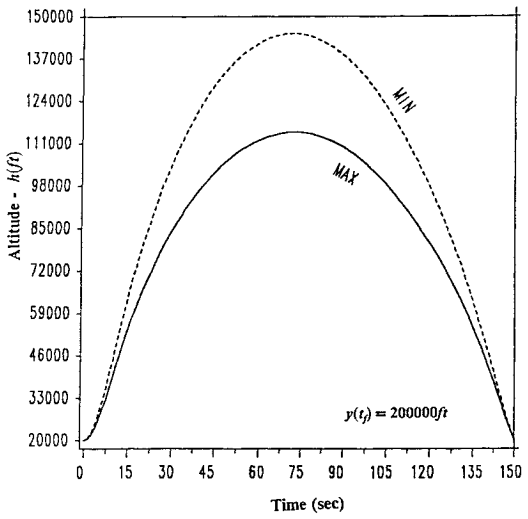

Fig. 8 Altitude time history.

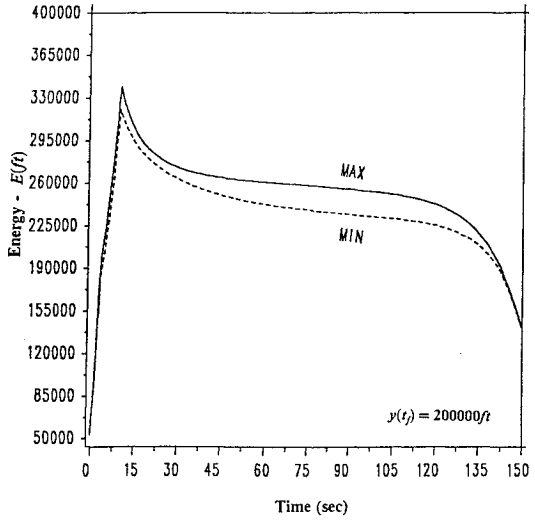

Fig. 9 Energy time history.

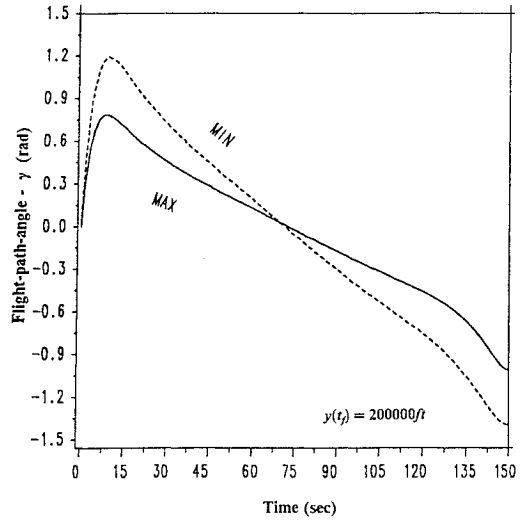

Fig. 10 Flight-path angle time history.

boundary conditions stated. The cross-range and heading angle histories shown in Figs. 7 and 11 show the missile turning left initially followed by a right turn for the minimum-range trajectory. Observe from Fig. 8 that the altitude values along the minimum-down-range path exceed those along the maximum-down-range path. Intuitively, this enables the missile to reduce the horizontal component of velocity while maintaining sufficient energy. The minimum-range trajectories must not be misinterpreted as energy-wasting trajectories.

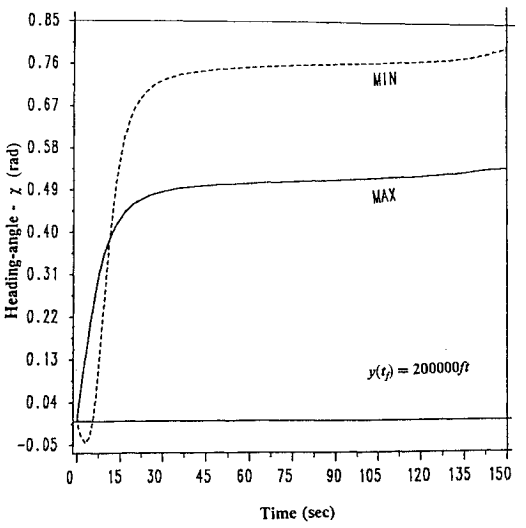

Fig. 11 Heading angle time history.

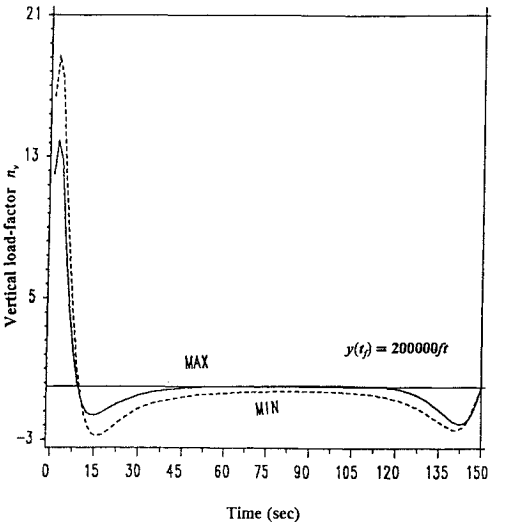

Fig. 12 Vertical load factor time history.

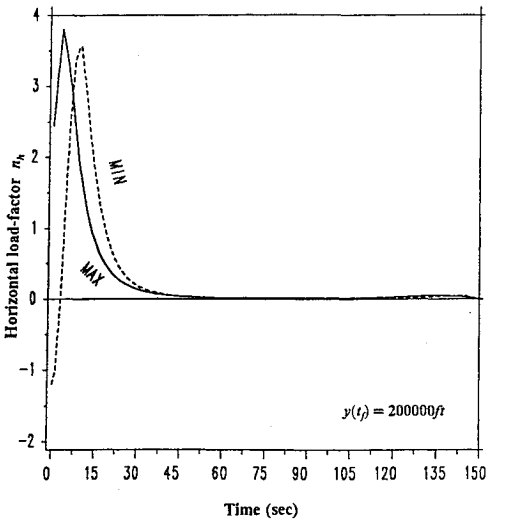

Fig. 13 Horizontal load factor time history.

The costate λ_E remains negative for all the minimum-range trajectories; hence these *are* energy conservative.

Necessary and Sufficient Conditions

Necessary Conditions

The second-order necessary conditions for a weak local minima are as follows:

1) There exists a weak form of the Legendre–Clebsch condition; i.e., for a minimizing extremal, $H_{uu} \geq 0$ for all $t_0 \leq t \leq t_f$.

2) If the former is true all along the candidate trajectory in the strong form, $H_{uu} \geq 0$, then the Jacobi condition[8] in the weakened form must be satisfied; i.e., the interval $t_0 \leq t \leq t_f$ must not contain any point conjugate[8] to $X(t_f)$.

It should be noted here that the above necessary conditions apply to extremals without corners. The necessary condition[15] that the regular extremal must have no conjugate points is only true for regular extremals without corners. The continuity of certain matrices for the accessory minimum problem is required in proving the necessary conditions. In the presence of corners, this continuity is not guaranteed. It is however necessary that no conjugate points (with respect to t_f) exist from final time backward to the time where a corner appears, i.e., the thrust switch from sustain to coast.

Sufficiency Conditions

The sufficiency conditions for a weak local minimum for problem $\boldsymbol{p}_1$ are given by Eqs. (16–18). They are strengthened forms of the above necessary conditions, assuming the problem to be normal.[8] Normality simply implies that the Euler–Lagrange equations satisfying the boundary conditions are not the only solution to the dynamic system. The specific example $\boldsymbol{p}_1$ has corners due to thrust switching. The costate multipliers are continuous across the corners, which occur at fixed time. For regular extremals with such corners the sufficiency conditions hold in the same sense as for a smooth extremal.

The sufficiency conditions[8] for problem $\boldsymbol{p}_1$ are

$$[H_{uu}] \geq 0 \quad \text{for} \quad t_0 \leq t \leq t_f \tag{16}$$

$$Q < 0 \quad \text{for} \quad t_0 \leq t < t_f \tag{17}$$

$$S - RQ^{-1}R^T \text{ finite} \quad \text{for} \quad t_0 \leq t \leq t_f \tag{18}$$

These three conditions correspond to the strengthened Legendre–Clebsch condition, normality condition, and the no-conjugate-point condition, respectively. The differential equations and boundary conditions governing S, Q, and R are as follows:

$$\dot{S} = -SA - A^T S + SBS - C \qquad S(t_f) = S_f \tag{19}$$

$$\dot{Q} = R^T B R \qquad Q(t_f) = 0 \tag{20}$$

$$\dot{R} = -(A^T - SB)R \qquad R(t_f) = R_f \tag{21}$$

The definition and notation of matrices A, B, C of the accessory minimum problem[8] and the boundary conditions in Eqs. (19–21) have been adopted from standard literature.[8] These are not repeated in this paper for the sake of conciseness.

It is possible during the testing of condition (18) that the matrix $S - RQ^{-1}R^T$ remains finite but its components S and $RQ^{-1}R^T$ become infinite. This is illustrated by a simple example (Ref. 8, example 2, p. 186). Analytically, this does not indicate nonoptimality of the reference trajectory under investigation. However, numerically, the no-conjugate-point test becomes impossible.

Suitably, the derivation to be followed aims at obtaining a differential equation and suitable boundary conditions for the test matrix itself. Define a matrix $Z = S - RQ^{-1}R^T$. This matrix Z is not defined at the final time of the test extremal, since $Q(t_f) = [0]$ and hence is singular. This new matrix is hence introduced from, $t_f - \varepsilon$, the choice of ε being arbitrarily small. The absence of conjugate points at t_f is obvious. Otherwise, the Jacobian associated with the TPBVP would be singular and a converged nominal solution would not be obtained in the first place.

The derivation of the matrix differential equation governing Z is performed by formally differentiating Z and using suitable substitutions as shown below:

$$\dot{Z} = \dot{S} - \dot{R}Q^{-1}R^T - R(\dot{Q}^{-1})R^T - RQ^{-1}\dot{R}^T \tag{22}$$

The four terms on the right-hand side (RHS) of above equation are treated separately as shown.

Below utilizing differential Eqs. (19–21) and the definition of the matrix Z, i.e., $S = Z + RQ^{-1}R^T$, the first term takes the form

$$\dot{S} = -ZA - RQ^{-1}R^T A - A^T Z - A^T RQ^{-1}R^T + ZBZ + RQ^{-1}R^T BZ + ZBRQ^{-1}R^T + RQ^{-1}R^T BRQ^{-1}R^T - C \tag{23}$$

The second term can be written as

$$-\dot{R}Q^{-1}R^T = A^T RQ^{-1}R^T - ZBRQ^{-1}R^T - RQ^{-1}R^T BRQ^{-1}R^T \tag{24}$$

The third term in Eq. (22) requires the first time derivative of Q^{-1}:

$$\frac{\mathrm{d}}{\mathrm{d}t}[I] = [0] \Rightarrow \frac{\mathrm{d}}{\mathrm{d}t}[QQ^{-1}] = [0] \Rightarrow \frac{\mathrm{d}}{\mathrm{d}t}[Q^{-1}] = -Q^{-1}\dot{Q}Q^{-1}$$

Thus the third term can be expressed as

$$-R(\dot{Q}^{-1})R^T = RQ^{-1}R^T BRQ^{-1}R^T \tag{25}$$

Using the fact that the matrices S and B are symmetric, the final term of Eq. (22) takes the form

$$-R(Q^{-1})\dot{R}^T = RQ^{-1}R^T A - RQ^{-1}R^T BZ - RQ^{-1}R^T BRQ^{-1}R^T \tag{26}$$

Adding up all four terms and canceling opposite terms, it can be easily shown that the matrix Z satisfies the matrix differential equation

$$\dot{Z} = -ZA - A^T Z + ZBZ - C \tag{27}$$

A necessary condition for no conjugate point on the extremal is that $Z(t)$ be finite for all $t_0 \leq t < t_f$. The scheme for testing for conjugate points involves integrating backward in time the differential Eqs. (19–21) for S, Q, and R from t_f to $t_f - \varepsilon$, where ε is an arbitrarily small time step. Evaluate $Z(t_f - \varepsilon)$ and integrate backward in time Eq. (27) and check the finiteness of Z. A similar differential equation is derived[16] for the problem $\boldsymbol{p}_2$ also.

Regularization

It is observed that sufficiency conditions require the Legendre–Clebsch condition in the strengthened form all along the extremal for $t_0 \leq t \leq t_f$. For extremals corresponding to the specific problem of range maximization/minimization or the equivalent time optimal problem, if the heading angle and flight-path angle at final time is unspecified, then the associated costate variables at final time are zero by transversality conditions. By Eqs. (12) and (13) this implies that both the controls n_v and n_h simultaneously vanish at the final time. The matrix H_{uu} becomes singular and makes the extremal nonregular. For such extremals, the conjugate point testing cannot be performed in the usual sense and a weak local minima cannot be established.

In a trial to overcome this problem, regularization of extremals are attempted by augmenting the performance index[17] of the original problem $\boldsymbol{p}_1$ as follows:

$$J = x(t_f) + \varepsilon_1 \gamma(t_f) + \varepsilon_2 \chi(t_f) \tag{28}$$

where the ε_i, $i = 1, 2$, are small quantities, not both zero. The term $x(t_f)$ may also be replaced by $y(t_f)$ depending upon the region of homotopy. This ensures that at least one of the controls is nonzero at final time, yielding H_{uu} matrix positive definite at final time, irrespective of the sign of ε_i. It is observed that for the flight in the vertical plane[4] the vanishing of the matrix H_{uu} can also happen for $t_0 \leq t < t_f$. Thus, these problems can be regularized by using $\varepsilon_2 \neq 0$. It has also been observed, that for three-dimensional flight the vanishing of the matrix H_{uu} in the interior of the time domain requires that two continuously varying costate variables λ_γ and λ_χ change sign at the same time. If this happens, then the cross over can be made nonsimultaneous by a careful selection of ε_i.

Once the problem is regularized, one checks the Jacobi condition using the method detailed earlier. It has been observed that the nonregular TPBVP solved using BOUNDSCO yields a solution within prescribed error tolerance. The transversality conditions $\lambda_\gamma(t_f) = 0$

and $\lambda_\chi(t_f) = 0$ are used for the problem with the final angles free. The solution yields values $\lambda_\gamma(t_f) = \delta_1$ and $\lambda_\chi(t_f) = \delta_2$, the δ_i of order 1.0×10^{-14}. If these values of δ_i are used as the values of ε_i, $i = 1, 2$, for the regularized problem and if the regularized TPBVP is re-solved, it would yield the same range $[x(t_f)$ or $y(t_f)]$ within prescribed tolerance. This is due to the limitation of numerical precision of the computations. The conjugate point test can be performed for this extremal, and one can establish a weak local minimum for the regularized extremal. Thus, one can abandon the "old" nonregular extremal in favor of the "new" regularized extremal, with identical (numerically) cost of range and check sufficiency conditions. It is clear that the sufficiency holds only for the regularized extremal and not the original nonregular extremal. Numerical tests for trajectories leading to the boundary of attainability were performed and absence of conjugate points established for regular and regularized extremals.

In theory, for the regular or regularized problem, the sufficiency conditions imply the existence of a local field about the test extremal. The existence of such a field about a nonregular extremal using classical theory is not proven. Even though one can show that there exists a field about the extremal with some $\varepsilon_i \to 0$ with $\varepsilon_i \neq 0$, one has to prove that this field does not collapse onto the extremal for both $\varepsilon_i = 0$. Conjugate point testing for irregular extremals may be performed using computational Jacobi procedures.[18] However, the absence of conjugate points along the test extremal does not imply the existence of a local field about the nonregular extremal.

Conclusions

Open-loop trajectories leading to the boundary of attainability of the missile are obtained. A comparison of the trajectories leading to maximum- and minimum-range boundaries are made. Typical maximum-range trajectories show initial maneuvers of large control efforts, quickly increasing flight-path angle and hence altitude, and aligning the heading to the final intercept point. A ballistic midcourse is observed for the missile-maximizing range. A typical proportional navigation scheme would cause the missile to "run out of steam" since the missile would operate at low altitude and hence experience high drag.

The necessary and sufficient conditions for optimality of sample trajectories were checked and were found to be satisfied. Regularization procedures to obtain sufficiency for a weak local minima and their limitations are also discussed. A matrix Z, its *new* governing matrix differential equation, and boundary conditions have been derived and used successfully to confirm absence of conjugate points in candidate regular and regularized extremals leading to the boundary of attainability sets.

The attainability sets for different fixed final times and the homotopy methods used to obtain them are interesting. The appearance of holes in the attainability sets and the nature of the boundary of these sets give insight to the range capabilities of the missile in atmospheric flight. Range charts for different boundary conditions derived by re-solving the TPBVP off-line can be used for real-time selection of nominal optimal intercept trajectories. An accompanying paper[5] deals with the closed-loop guidance of this missile against a maneuvering target.

Acknowledgments

This work was supported in part by Air Force Armament Laboratory, Eglin AFB, under contract F08635-86-K-0390 and in part by DARPA under contract (ACMP) F49620-87-C-0116.

References

[1]Cheng, V. H. L., and Gupta, N. K., "Advanced Midcourse Guidance for Air-to-Air Missiles," *Journal of Guidance, Control, and Dynamics*, Vol. 9, No. 2, 1986, pp. 135–142.

[2]Menon, P. K. A., and Briggs, M. M., " A Midcourse Guidance Law for Air-to-Air Missiles," *Proceedings of the AIAA Guidance, Navigation, and Control Conference*, AIAA, Washington, DC, 1986 (AIAA Paper 87-2509).

[3]Cheng, V. H. L., Menon, P. K. A., Gupta, N. K., and Briggs, M. M., "Reduced-Order Pulse-Motor Ignition Control Logic," *Journal of Guidance, Control, and Dynamics*, Vol. 10, No. 4, 1987, pp. 343–350.

[4]Katzir, S., "Optimal and On-Board Near-Optimal Midcourse Guidance," Ph.D. Dissertation, Virginia Polytechnic Inst. and State Univ., Blacksburg, VA, Nov. 1988.

[5]Kumar, R. R., Seywald, H., and Cliff, E. M., "Near Optimal 3-D Guidance Against a Maneuvering Target," *Proceedings of the AIAA Guidance, Navigation, and Control Conference*, AIAA, Washington, DC, 1989 (AIAA Paper 89-3480).

[6]Visser, H. G., "Energy Management of Three-Dimensional Minimum-Time Intercept," Ph.D. Dissertation, Virginia Polytechnic Inst. and State Univ., Blacksburg, VA, Aug. 1985.

[7]Bulirsch, R., "Die Mehrzielmethode zur numerischen Losung von nichtlinearen Randwertproblemen und Aufgaben der optimalen Steuerung," *Lehrgang Flugbahnoptimierung Carl-Cranz-Cessellschaft e.v.*, Oct. 1971.

[8]Bryson, A. E., and Ho, Y. C., "Applied Optimal Control," Hemisphere, New York, 1975, Chap. 6, pp. 177–202.

[9]Pontryagin, L. S., Boltyanskii, V. G., Gamkrelidze, R. V., and Mischenko, E. F., *The Mathematical Theory of Optimal Processes*, Wiley-Interscience, New York, 1962.

[10]Leitman, G., *An Introduction to Optimal Control*, McGraw-Hill, New York, 1966.

[11]Lee, E. B., and Markus, L., *Foundations of Optimal Control Theory*, Krieger, Malabar, FL, 1986.

[12]Marec, J. P., *Optimal Space Trajectories*, Elsevier, New York, 1979.

[13]Vinh, N. X., *Optimal Trajectories in Atmospheric Flight*, Elsevier, New York, 1981.

[14]Hermes, H., and LaSalle, J. P., *Mathematics in Science and Engineering*, New York, Academic Press, 1969, Vol. 56.

[15]Breakwell, J. V., and Ho, Y. C., "On the Conjugate Point Condition for the Control Problem," *International Journal of Engineering and Science*, Vol. 2, 1965, pp. 565–579.

[16]Kumar, R. R., "Optimal and Near-Optimal Medium Range Air-to-Air Missile Guidance Against Maneuvering Targets," Ph.D. Dissertation, Virginia Polytechnic Inst. and State Univ., Blacksburg, VA, June 1989.

[17]Ewing, G. M., *Calculus of Variations with Applications*, Dover, New York, 1985.

[18]Kelley, H. J., and Moyer, H. G., "Computational Jacobi-Test Procedure," *Proceedings of Workshop: Current Trends in Control*, JUREMA, Zagreb, Yugoslavia, 1985.